Characterising the importance of porosity of large woody debris accumulations at single bridge piers on localised scour

D. Panici[1], and P. Kripakaran[2]

[1]Centre for Resilience in Environment, Water and Waste (CREWW), Faculty of Environment, Science and the Economy, University of Exeter, Exeter, United Kingdom
[2]Department of Engineering, Faculty of Environment, Science and the Economy, University of Exeter, Exeter, United Kingdom

Key Points:

- Accumulations of large woody debris (LWD) can increase scour depths at bridge piers by a factor of up to three
- The porosity of LWD accumulations may reduce up to 50% the size and depth of scour holes estimated with solid LWD
- A functional relationship for measured laboratory data is proposed to estimate the reduction in scour depth due to the porosity of LWD accumulations

Corresponding author: Diego Panici, d.panici@exeter.ac.uk

Abstract

The accumulation of large woody debris (LWD) at bridge piers is a serious hazard to the structural integrity of bridges across watercourses worldwide. The exacerbated scour that can directly result from LWD accumulations can lead to major structural damage or even catastrophic collapse. Recent research has led to empirical equations to estimate the scour depth for given LWD accumulation size; however these are mostly based on experimental tests with prismatic and impervious solid LWD accumulations, ignoring field observations that have shown that accumulations are neither impervious nor prismatic but are porous with inverted conical shapes. In this study, we therefore investigate the effects of porous LWD accumulations having shapes commonly observed in the field on scour holes. Results reveal that LWD size and shape, and flow characteristics are the primary factors influencing the erosion of sediments at the base of bridge piers. However, the porosity of accumulations is also observed to have a considerable effect on the size and maximum depth of scour holes. In particular, porous LWD reduce the maximum scour depth by up to 50% (and on average in the range of 5-25%) relative to the respective solid impervious accumulation. The results shown in this study also provide a practical tool for arriving at more realistic and less conservative estimates of scour depths at bridge piers when affected by LWD accumulations.

1 Introduction

Localised scour at bridge piers is generally regarded as the main structural threat for bridges over water. For this reason, a substantial amount of literature has documented the catastrophic impacts that scour can have on the stability of bridges (e.g. *Benn*, 2013). Although large woody debris, LWD, as used in this paper and within the bridge engineering community (or simply large wood as increasingly referred to within the water resources community where other waterborne elements like microplastics can constitute debris) has been recognised as a crucial resource for river restoration and natural flood management (*Wohl et al.*, 2019; *Gurnell et al.*, 2019), many studies in the last century have reported substantial evidence that LWD accumulations at bridge piers can greatly exacerbate scour. For example, up to 30% of bridge failures due to hydraulic actions in the UK, US and Ireland are directly linked to LWD accumulations (*Diehl*, 1997; *Benn*, 2013).

In general, LWD accumulations at bridge piers may occur as single logs, large accumulations or a complete span blockage (*Diehl*, 1997; *Lagasse et al.*, 2010; *Lyn et al.*, 2007; *Panici et al.*, 2020; *Panici and Kripakaran*, 2022); however, the most common field observation for the majority of the bridge piers affected by LWD is a single accumulation (*Diehl*, 1997; *Panici et al.*, 2020; *Panici and Kripakaran*, 2022) for which the typical shape is an inverted half-cone (*Diehl*, 1997; *Lagasse et al.*, 2010). Experimental observations (*Panici and de Almeida*, 2018; *Parola et al.*, 2000; *Panici and de Almeida*, 2020a) have confirmed this recurring shape, and have also shown that the maximum size of such accumulations can be estimated based on flow and LWD properties (*Panici and de Almeida*, 2018). The obstruction caused by accumulated LWD results in a constriction of the flow at the pier section, which increases flow velocity and consequently the turbulent vorticity system around the pier (*Pagliara and Carnacina*, 2013), both of which worsen scour.

The quantification of the increase in scour depth due to LWD accumulations has been the object of several studies in the last few decades, even though these were mostly based on laboratory scale experiments due to the complex nature of the phenomena and the difficulty to collect measurements in flood conditions. In one of the earliest experimental studies on the topic, *Laursen and Toch* (1956) showed that LWD accumulations made of twigs and sticks would produce scour holes that are deeper and larger than unobstructed piers. This observation was confirmed by *Melville and Dongol* (1992) who experimentally studied the contribution of LWD to local scour using the approach of the equivalent pier (i.e. the effective diameter of the pier necessary to produce the same scour hole); they represented LWD accumulations using regular shapes (i.e. cylinders and cones) installed at the top of the pier. *Pagliara and Carnacina* (2010), *Pagliara and Carnacina* (2011) and *Pagliara and Carnacina* (2013) employed rectangular shapes for LWD accumulations, and also utilising the work by *Melville and Dongol* (1992), refined the *equivalent pier* methodology and tested different LWD size, position, and characteristics including roughness and porosity. LWD roughness was also the focus of the investigation by *Lagasse et al.* (2010), who used a wedge-shaped solid with protruding spikes. *Ebrahimi et al.* (2018) carried out a series of experimental tests by testing different shapes (e.g. cylindrical log, wedge) and vertical positions (e.g. at the water surface, on the flume bed) of LWD jams, whilst *Cantero-Chinchilla et al.* (2021) investigated the formation of the scour hole when the size of LWD accumulations is dependent, by using a functional relationship (*Panici and de Almeida*, 2018), on flow and LWD values.

Results from these experimental works highlighted that the impact of LWD accumulations on the formation of the scour hole is substantial. In all cases, a considerable increase in scour depths and volume was observed, up to 3 times the maximum depth without LWD (*Ebrahimi et al.*, 2018; *Pagliara and Carnacina*, 2010). Moreover, the size of the LWD jams was also noted as a key factor influencing the scour hole, with larger jams producing deeper and wider holes (*Ebrahimi et al.*, 2018; *Lagasse et al.*, 2010). Related parameters that were also observed to play an important role were the obstructed area (*Lagasse et al.*, 2010; *Ebrahimi et al.*, 2018) and the relative water depth (i.e. the free depth beneath the LWD accumulation at the pier section) (*Ebrahimi et al.*, 2018, 2020), both of which are measures of the constriction of the flow caused by LWD (*Pagliara and Carnacina*, 2013). Furthermore, experimental tests by *Pagliara and Carnacina* (2010) indicated that roughness may have a notable effect on the overall scour (that is, coarser accumulations will cause larger scour holes). Nevertheless, tests by *Lagasse et al.* (2010) suggested that roughness only has second-order effects, which is in contrast with findings by *Pagliara and Carnacina* (2010).

In this context, two crucial aspects strongly affecting the scour phenomena have been relatively overlooked.

1. The majority of past studies mimicked LWD accumulations using prismatic shapes (e.g. cuboids), which do not reflect real-world observations. This is a major limitation, since the LWD shape (*Pagliara and Carnacina*, 2010; *Ebrahimi et al.*, 2018; *Cantero-Chinchilla et al.*, 2021) has been found to be a critical factor in the formation of the scour hole as it affects significantly the change in flow around the pier.
2. Another parameter that has only been marginally investigated so far is the porosity of the LWD accumulation. Most studies focused on impervious LWD jams; these studies potentially overestimated the effects of LWD on scour, since *Parola et al.* (2000) showed that porosity can have a great importance on the drag force applied to LWD at bridge piers. *Pagliara and Carnacina* (2010) tested scour at single bridge piers with LWD using two values of porosity (namely 0 and 0.6) and found that temporal evolution was similar across experimental tests. On the other hand, the scour depths due to LWD accumulations at a full-channel width array of piers were shown to be highly dependent on the solid volume occupied by LWD, and thus its porosity (*Schalko et al.*, 2019). Since the role of porosity of LWD accumulations at single bridge piers has yet to be fully investigated, it is currently impossible to quantify the change in scour depth and volume that this can cause, compared to fully impervious LWD accumulations, on which most of the available literature is based.

This study will address these two limitations.

The aim of this study is to investigate the importance of porosity of LWD accumulations on the formation of scour holes at bridge piers with realistic (not idealised, such as cylinders or cuboids) LWD shapes. To this end, we carried out an exhaustive ex-

Table 1. Flow scenarios for the experimental tests carried out in this work.

Flow scenario	**Discharge (m^3/s)**	**Water depth (m)**	**Velocity (m/s)**	*Fr*
a	0.0206	0.120	0.281	0.259
b	0.0266	0.120	0.363	0.335
c	0.0306	0.120	0.418	0.385

perimental campaign testing several values of LWD porosity and accumulation sizes, and mapped the resulting scour hole formed at a model bridge pier. The observations and analysis in this work will pave the way for the inclusion of the effects of LWD porosity on the evaluation of scour at bridge piers prone to LWD accumulations.

2 Methodology

We conducted an experimental campaign at the University of Exeter using a large glass-walled recirculating flume, 0.61 m wide, 14 m long and 0.70 m deep. Figure 1 shows a sketch of the flume and the experimental set-up, as well as a picture illustrating the pier setting and a few examples of the large wood jams used. The flume was kept horizontal and a layer of sediment with a thickness of 0.22 m was placed on the flume bed. Furthermore, gravel pits were placed at both inlet and outlet to attenuate any removal of sand from the flow by potentially high turbulence at these locations, whilst flow straighteners were placed at the flume inlet to suppress excess turbulence and secondary currents. The water depth in the flume h was controlled by a tilting flap gate at the flume outlet, and was kept constant for all experimental tests at 0.12 m. Since the main purpose of this work was to understand how the porosity of LWD affects scour development, the variation of water depth on the scour depth was not investigated. Water discharge was controlled through a magnetic flow meter (nominal accuracy 0.5%) and three different flow rates were tested, namely 0.0206 m^3/s, 0.0266 m^3/s and 0.0306 m^3/s. These flow discharges correspond to average flow velocities v of 0.281 m/s, 0.363 m/s and 0.418 m/s, and Froude number Fr of 0.259, 0.335 and 0.385, respectively, which are typical for flood flows in lowland rivers. Table 1 summarises the different flow scenarios (named a, b, and c) that have been used for this work. For all experimental tests, a model bridge pier was placed at the flume centreline and attached to the flume bed. The pier was chosen as a triangular sharp nose type, with two cutwaters (front and rear) and an elongated straight section; this geometry is very common amongst masonry bridge piers, which constitute a large portion of scour-prone bridge piers in the UK and Europe. The front tip of the model pier was placed 5.5 m downstream of the flume inlet. The pier width was chosen as 50 mm, the overall length 206 mm, and the cutwater had an angle of 90° at both front and rear ends. Figure 1 also shows the coordinate system used in this work; x is taken streamwise along the flume centreline, y is transverse and perpendicular to the flow and z is vertically upward. The origin of the coordinate system is assumed to be at the flume centreline and 25 mm from the upstream sharp nose of the pier (as shown in Figure 1), with z=0 corresponding to the initial uneroded bed level at the start of an experimental run.

The type of sediment used for the experimental campaign was dry silica sand, with size varying between 1.0 and 2.0 mm. The median size of sediment material d_{50} was measured as 1.37 mm, whilst the uniformity coefficient d_{60}/d_{10} was 1.36, and the geometric standard deviation of sediment particle size distribution σ_g=d_{84}/d_{50} was equal to 1.21. This size distribution was particularly suitable for experimental tests, since: i) bed forms are unlikely to be observed in undisturbed flows for d_{50} $\geq$0.8 mm (*Oliveto and Hager*, 2005); ii) ripples are unlikely to form if σ_g $\leq$1.5 (*Raudkivi and Ettema*, 1983); iii) armouring effect can be neglected if σ_g $\leq$1.30 (*Raudkivi and Ettema*, 1985); iv) clear water conditions are prevalent due to velocity being below critical velocity (according to

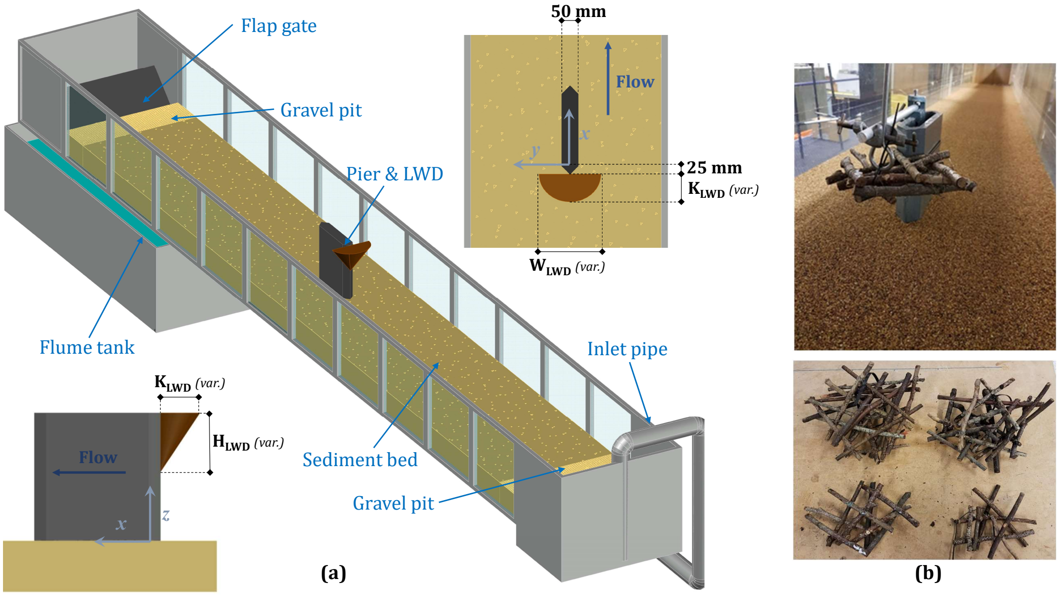

Figure 1. (a) Sketch of the flume and experimental set-up, with indication of the pier, LWD jam, and coordinate system, and a plan view and a side view of the area surrounding the pier, where the coordinate system is shown in the plan and elevation views; figure not to scale. (b) An example of a LWD jam from experimental group B1 attached to the model pier (top) and pictures of the LWD jams used for experimental groups A2, B1, C1 and D2 (bottom) (see Table 2 for details on the LWD jams).

e.g. *Neill*, 1968; *Garde*, 1970) and no sediment influx; and v) sediment size distribution was essentially uniform.

LWD accumulations were chosen to have a half-conical shape, based on experimental observations (*Panici and de Almeida*, 2018; *Parola et al.*, 2000; *Panici and de Almeida*, 2020a), field analysis and photographic evidence (*Diehl*, 1997; *Lagasse et al.*, 2010; *Lyn et al.*, 2007), and available satellite imagery (*Panici et al.*, 2020; *Panici and Kripakaran*, 2022). As in previous studies (*Pagliara and Carnacina*, 2010; *Cantero-Chinchilla et al.*, 2021), the LWD jams tested in this work were also made of natural sticks glued together to mimic real-world LWD accumulations. For each experiment, the LWD inverted half-cones were clamped to the bridge pier and completely submerged at all times, placing the LWD top flat surface in correspondence of the free flow surface. Four different LWD accumulation geometries were chosen (named as types A, B, C and D, from smallest to largest). The dimensions of each of the accumulation geometries were measured. The width W_{LWD} and length K_{LWD} were measured in accordance with the plan view in Figure 1. The height H_{LWD} was measured as the overall height of the accumulation from its lower end to the top surface, according to the side view in Figure 1. For each tested accumulation, there was always a gap between the lower end of the LWD jam and the flume bed, to reflect real-life observations (*Lagasse et al.*, 2010) of accumulations typically floating above the river bed. Furthermore, for each of the LWD accumulation geometries, different values of porosity were tested. For the purpose of this work, porosity p is herewith defined as:

$$p = \frac{V_v}{V_t} \tag{1}$$

where V_v is the volume occupied by water within the theoretical total volume of the half-cone shape V_t. V_v was computed as V_v=V_t-V_{LWD} where V_{LWD} represents the total LWD volume, which was measured by estimating the change in water level (and therefore in volume) of a graduated bucket filled with water when each LWD size was immersed. Consequently, the porosity p can be written in terms of V_{LWD} and V_t as follows:

$$p = 1 - \frac{V_{LWD}}{V_t} \tag{2}$$

For this experimental work, the values of porosity were chosen in the range 0.167 - 0.780 (with the addition of the impervious case, for which p=0). Such broad range reflects the inherent variability that can be observed in real-world jams. For example, *Livers et al.* (2020) observed porosity values in several riverine locations in North America in the range 0.18 - 0.88 (depending on sorting and organisational structure) which are consistent with the porosity of LWD jams tested in this work. Different porosity values were obtained by changing the internal structure of the LWD jam (although keeping the external size the same for all same-size tests); for $p = 0$, the accumulation was wrapped with thin waterproof material in order to keep shape and roughness consistent with the other tests while obtaining an impermeable solid.

Table 2 shows the size and porosity values of each LWD size employed for this work. For each combination of LWD accumulation geometry and porosity, experiments were conducted for the three flow scenarios given in Table 1, where each scenario has a unique Fr value. In Table 2, the test labels are arrived at by combining the labels for the accumulation geometry, the porosity, and the flow scenario in that order. The labels for the accumulation geometries are A, B, C and D, in order of increasing size, as defined in Table 2. The porosity label for a LWD size corresponds to the rank (e.g. 1, 2, etc.) of the LWD accumulation's porosity value p when the tested porosity values for that LWD size are arranged in decreasing order, with the highest rank (1) corresponding to the highest porosity and the lowest rank corresponding to the impervious scenario ($p = 0$). The labels for the flow scenarios are as follows: a for Fr=0.259, b for Fr=0.335 and c for Fr=0.385, as specified in Table 1. Therefore, test A1b, for example, corresponds to the test with LWD size A having the highest porosity p=0.529 as shown in Table 2, and for flow scenario b (Fr=0.335). Furthermore, for each Fr, a pilot test without LWD accumulations was performed (referred to as Pa, Pb and Pc).

Before each test, the flume bed was carefully smoothed with a smoothing board having a spirit level, and bed depths were spot-checked with a digital point gauge. Each test was run as follows. First, the flume was carefully filled with water, then the pump was turned on and both flow rate and flow depth carefully adjusted gradually until reaching the target flow conditions. The duration of each experiment was set at 5 hours. This duration was chosen since it is expected to be sufficient to produce a scour depth exceeding 85% of the equilibrium scour depth (*Melville and Chiew*, 1999) for all tested scenarios. The same duration was also used in scour experiments wherein quasi-equilibrium state was attained for similar sediment and flow conditions in the same flume facility (*Ebrahimi et al.*, 2018). Furthermore, the aim of this experiment was not to measure the full equilibrium scour which would have required an impractically long experimental time (*Dey et al.*, 1995).

After 5 hours, the flow rate was gradually reduced to zero. The LWD jam was then removed and the depth of the scour hole was mapped using an ADV (accurate to ±0.1%) guided by a remote-controlled modular system fixed at constant height and moving across a x-y grid (accuracy 0.5 mm). The ADV was only used to measure the vertical distance between the receiver and the channel bed at the end of each experiment; no velocity measurements were collected. Where measurements were impractical with the ADV (e.g. immediately adjacent to the pier), the scour depth was measured using a ruler and a digital point gauge. It was assumed that the scour depths either side of the pier were symmetrical at the end of each experiment, due to the pier being placed along the flume centerline and the flow conditions also being symmetric either side of the pier. This assumption was initially verified for a few scour holes by mapping the scour holes on both sides of the pier, and the resulting differences between the two sides were always observed to be less than 5% of the measured depths on one side. Therefore for subsequent experiments, the scour depths were mapped on only one side of the pier.

3 Results

Figure 2 shows the scour map obtained at the end of test C1c as a representative example of the scour observed during the experiments. It has the typical features of scour at single bridge piers as has also been widely noted in the literature (e.g. *Melville and Dongol*, 1992; *Ebrahimi et al.*, 2018; *Pagliara and Carnacina*, 2010). For example, the upstream front is characterised by a circular arc with steep slopes, then followed by a milder (but longer) slope up to the far (downstream) end of the pier. In some cases, a dune formation was observed downstream of the pier.

In general, the presence of LWD accumulations at the model pier produced scour holes that were significantly larger than those in the absence of LWD (i.e., cases Pa, Pb and Pc), typically between 20% and 90%, but in some cases up to approximately 250%. Figures 3, 4 and 5 show the contour maps of experimental groups A and D side-by-side for $Fr = 0.259$, 0.335 and 0.385, respectively, as well as the contour maps for no-LWD scenarios (tests Pa, Pb and Pc). Experimental groups B and C have not been shown here, since they were tested for only one value of p in this work. In all cases, the maximum scour depth was observed at the corner of the cutwater, corresponding to coordinates $x = 0$ mm and $y = \pm 12.5$ mm. Furthermore, the figures clearly show that a decrease in porosity p corresponds to an increase in depth and size of the scour hole (except for tests A1a and A3a), with impervious LWD jams (i.e. $p = 0$) showing the widest and deepest scour holes. In a similar way, the size of LWD accumulations affects significantly

Table 2. Summary of tests conducted with respective LWD size and porosity, and Fr. Each test with LWD accumulation is named with a 3-character reference: the first character is one of A, B, C, and D, which denote the geometry (type) of LWD jam tested; the second is one of 1, 2, 3, and 4, which corresponds to the values of porosity tested for each LWD jam geometry in descending order; the third is one of a, b, and c referring to the value of Fr (see Table 1) used for each test. Tests Pa, Pb, and Pc are pilot tests without LWD accumulations.

Test name	Size of LWD			LWD porosity p	Fr
	Width W_{LWD} (mm)	Height H_{LWD} (mm)	Length K_{LWD} (mm)		
A1a					0.259
A1b				0.529	0.335
A1c					0.385
A2a					0.259
A2b				0.375	0.335
A2c	180	40	130		0.385
A3a					0.259
A3b				0.167	0.335
A3c					0.385
A4a					0.259
A4b				0	0.335
A4c					0.385
B1a					0.259
B1b	240	50	140	0.571	0.335
B1c					0.385
C1a					0.259
C1b	280	90	200	0.780	0.335
C1c					0.385
D1a					0.259
D1b				0.774	0.335
D1c					0.385
D2a					0.259
D2b				0.711	0.335
D2c	320	100	230		0.385
D3a					0.259
D3b				0.433	0.335
D3c					0.385
D4a					0.259
D4b				0	0.335
D4c					0.385
Pa					0.259
Pb	N/A	N/A	N/A	N/A	0.335
Pc					0.385

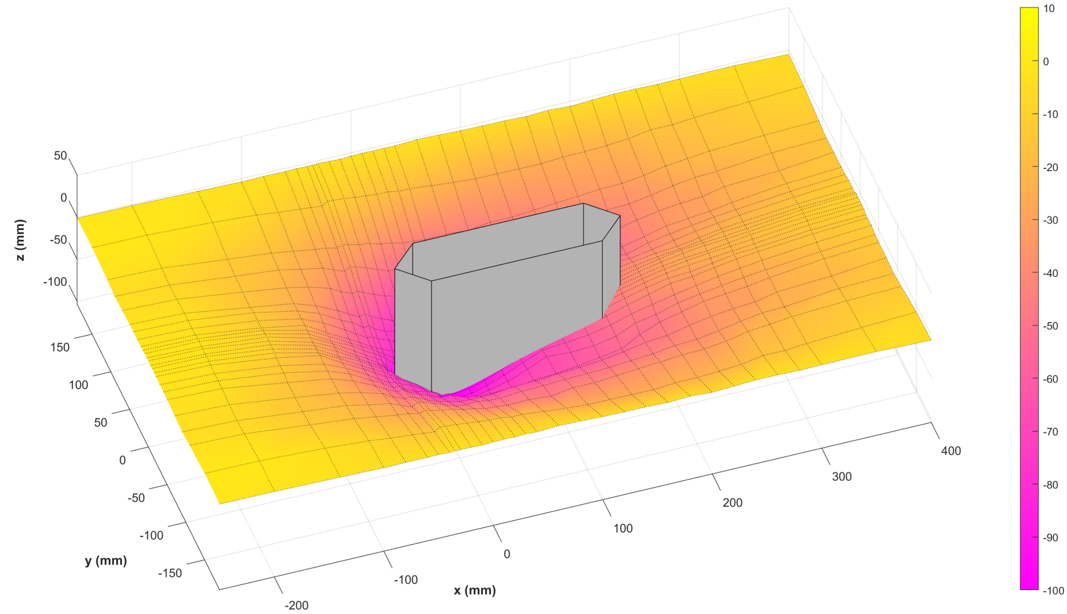

Figure 2. 3D mapping of the scour hole observed around the pier (grey solid) for experimental test C1c. Units are in mm. Origin of the coordinate system is located located according to Figure1

the resulting scour; the largest accumulation geometry (i.e. group D) led to much larger scour holes than the smallest (i.e. group A) for all cases. Also, when compared to the corresponding no-LWD cases, the overall increase in size of the scour hole is substantial, up to 3.5 times larger for test D4a.

Some geometric and geomorphic observations regarding size and location of the scour hole can be made for tests with the lowest Fr value ($Fr = 0.259$), results for which are shown in Figure 3. First, the scour hole extends over a smaller upstream (i.e., $x \leq 0$) area than observed in experimental tests with higher Fr values and for the case of the pier-only test Pa. Second, for all cases in Figure 3 (including the pier-only test), a dune is observed to form in the downstream section (i.e. $x \geq 0$), and the size of the dune increases with the scour hole size (i.e., with decreasing LWD porosity and increasing size of LWD). Also, the dune is observed to shift downstream as the size of the scour hole increases. For example, in test D4a (i.e., for the largest LWD accumulation with porosity $p = 0$), the dune is observed in the region $150<x<250$, while in test A1a (i.e., for the smallest LWD accumulation with the highest tested porosity $p = 0.529$) the dune is in the region $50<x<150$. The formation of the dune is however not observed for the two higher Fr values, for both with and without LWD.

Further insights can be obtained from the analysis of the longitudinal profiles of the scour holes, i.e., along the x direction. Figures 6 and 7 show the depth of scour along the line $y = 0$ for $x < -25$ mm and $x > 181$ mm, and along the outside of the pier for intermediate x values (i.e. -25 mm $\geq x \geq$ 181 mm) for LWD sizes A and D, respectively. The profiles present similar characteristics for different flow conditions and LWD porosity values. In all cases, the inclusion of LWD accumulations increases the depth and extent of the scour hole in all directions. At the same time, LWD porosity affects the depth and width of the scour hole, although in a non-linear way. For example, whilst the widest and deepest scour hole for each LWD size is observed for the impervious accumulation (i.e. $p = 0$ in tests A4a, A4b, A4c, D4a, D4b, D4c), the scour holes for LWD size A with porosity value of $p = 0.529$ (i.e., test A1c) were wider (≈550 mm) and deeper (92 mm) than those for accumulations with smaller values of p (e.g., for $p = 0.167$ the

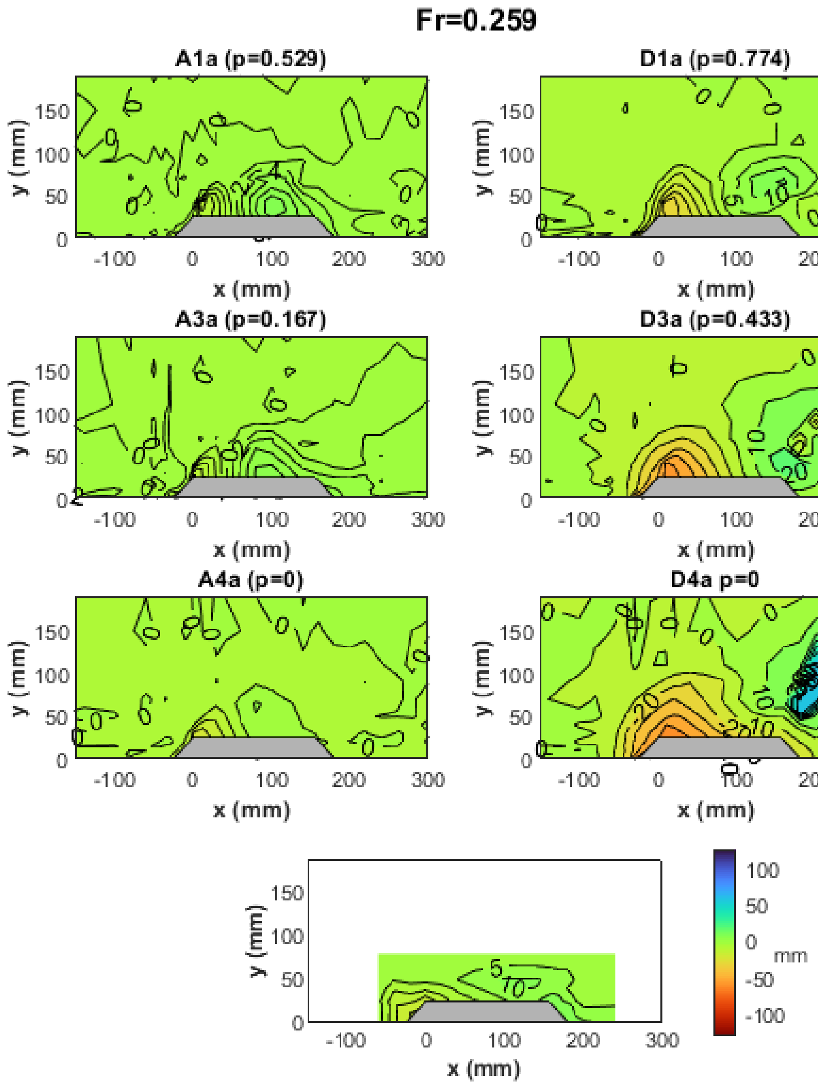

Figure 3. Scour contour maps obtained for tests A1a, A3a, A4a, D1a, D3a, D4a (where A corresponds to LWD with W_{LWD}=180 mm, H_{LWD}=40 mm, and K_{LWD}=130 mm, and D to W_{LWD}=320 mm, H_{LWD}=100 mm, and K_{LWD}=230 mm) and Pa (the corresponding no-LWD scenario). Fr=0.259 in all these tests. Dunes (of different heights and shapes) can be observed for all experiments for x >50 mm. Units are in mm.

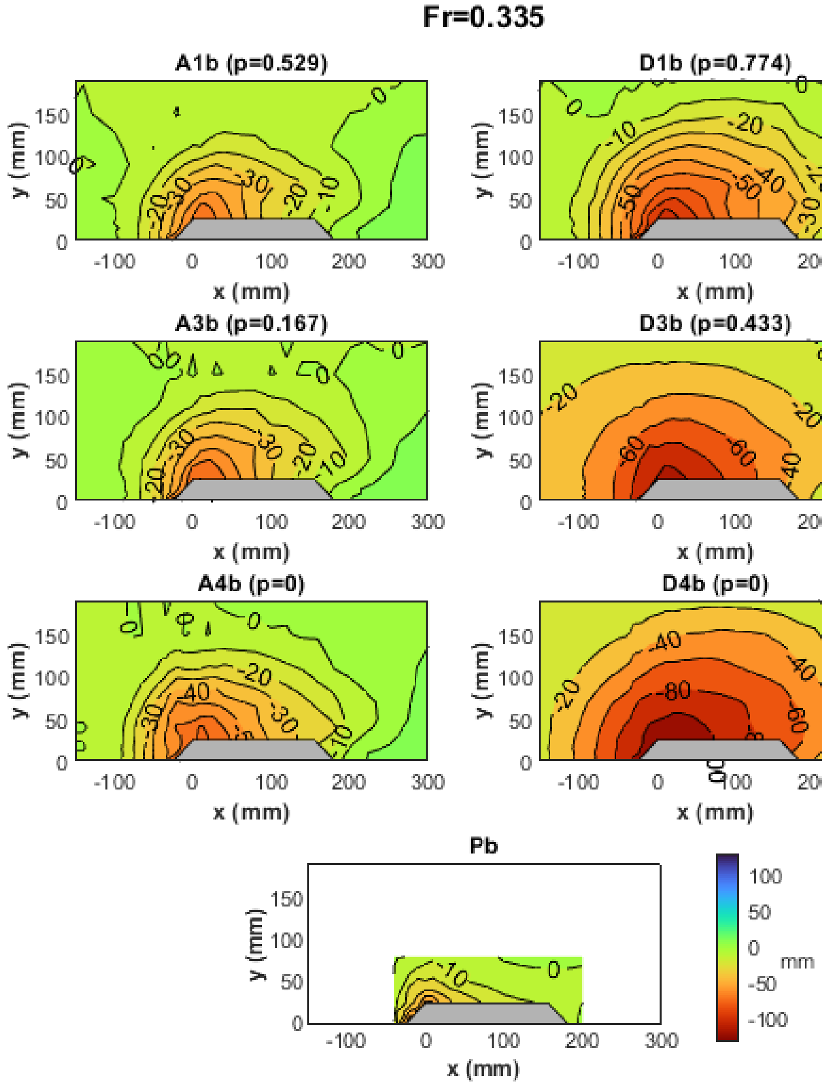

Figure 4. Scour contour maps obtained for tests A1b, A3b, A4b, D1b, D3b, D4b (where A corresponds to LWD with W_{LWD}=180 mm, H_{LWD}=40 mm, and K_{LWD}=130 mm, and D to W_{LWD}=320 mm, H_{LWD}=100 mm, and K_{LWD}=230 mm) and Pb (the corresponding no-LWD scenario). Fr=0.335 in all these tests. Units are in mm.

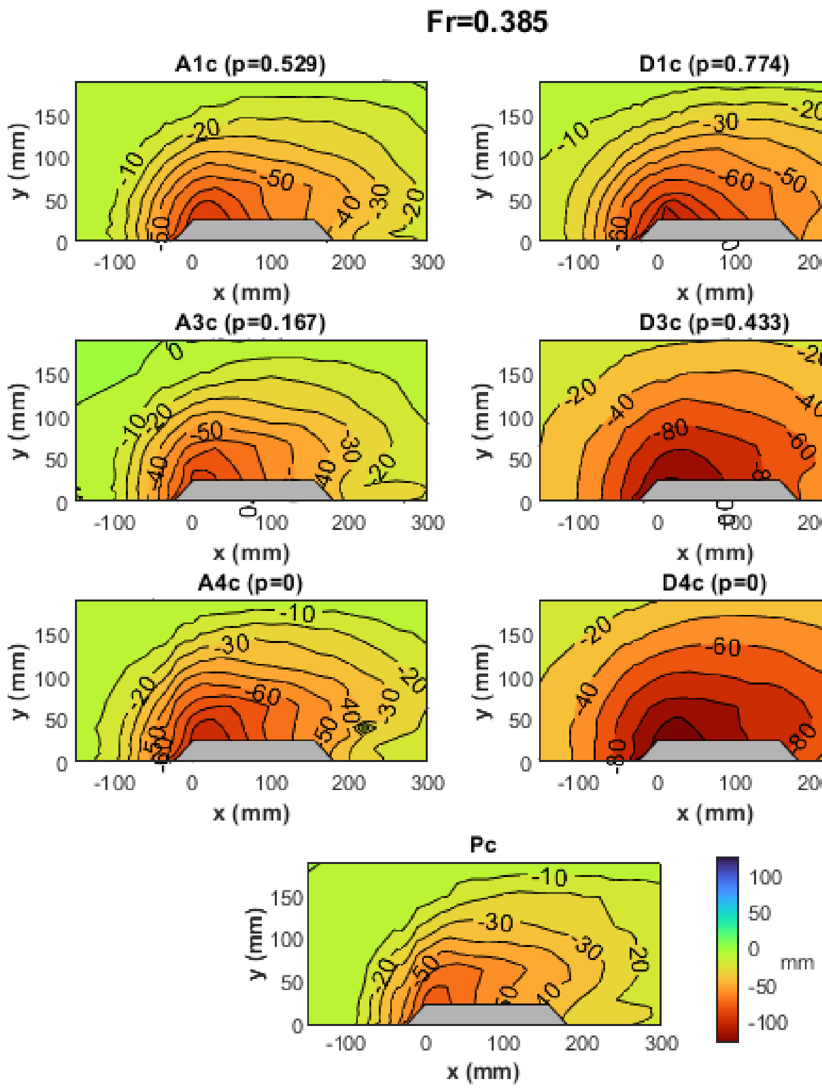

Figure 5. Scour contour maps obtained for tests A1c, A3c, A4c, D1c, D3c, D4c (where A corresponds to LWD with W_{LWD}=180 mm, H_{LWD}=40 mm, and K_{LWD}=130 mm, and D to W_{LWD}=320 mm, H_{LWD}=100 mm, and K_{LWD}=230 mm) and Pc (the corresponding no-LWD scenario). Fr=0.385 in all these tests. Units are in mm.

scour hole was ≈400 mm wide and 89 mm deep). On the other hand, the most porous LWD accumulations always produced the shallowest and shortest scour holes for each respective LWD type (other than the no-LWD tests). In general, the upstream slope of the scour hole along the x direction had gradients (as measured from the horizontal) between 34° and 38°, resulting in almost equal slopes across experimental tests, as seen in Figures 6 and 7. It is also observed that the upstream slope is typically steeper than the downstream slope, which averaged 18°. The contour plots also show that the location of the maximum scour depth shifts slightly (by up to 20 mm) in the downstream direction with increasing values of the maximum scour depth for the majority of the cases, except in a few tests such as for p=0.711 in Figure 4.

A final important inference can be drawn about the influence of LWD porosity on maximum scour depth. Figure 8 plots the maximum scour depth y_s (vertical axis) for each experimental test versus Fr (horizontal axis), whilst Figure 9 plots the relative scour depth d_r for LWD sizes A and D, i.e. the ratio between maximum scour depth for a scenario with $p > 0$ (i.e., $y_{s,eff}$) and the corresponding maximum depth for $p = 0$ (i.e., $y_{s,imp}$), computed as:

$$d_r = \frac{y_s(p > 0)}{y_s(p = 0)} = \frac{y_{s,eff}}{y_{s,imp}} \tag{3}$$

Consistent with the contour and profile observations, the effect of LWD porosity on maximum scour depth y_s is noticeable from Figures 8 and 9. Figure 8 also shows that LWD jams with $p = 0$ produced the deepest scour holes in all cases for each LWD size, with the only exceptions being test D4a, wherein $y_s = -50$ mm and test D3a, for which p=0.433, with $y_s = -52$ mm. Another observation is the importance of the LWD size for the absolute scour depth. The four geometries of LWD jams produced scour depths y_s that increased with increase in LWD size. Figure 8 shows that there is clearly a direct relationship between maximum scour depth, Fr, and LWD size. Nevertheless, this is not evident when examining only the relative scour depths d_r in Figure 9: when observing this dimensionless quantity, there is no clear distinction between results for different LWD sizes for each Fr value. Also, the effect of Fr is much less pronounced, especially for $Fr =$ 0.335 and $Fr =$ 0.385, for which the values of relative maximum scour depth are almost all contained within the interval 0.78 - 0.94. The situation is different for $Fr =$ 0.259, since the range of relative maximum scour depth is much wider (0.50 - 1.04), but there is still no clear tendency observed for the different sizes of LWD accumulations. Furthermore, $Fr = 0.259$ is the only flow condition for which the scour depth for a test with a porous LWD jam is greater than the non-porous case (specifically, for test D3a). On the other hand, also for $Fr = 0.259$, tests A1a and A3a were the only experiments that displayed maximum scour depths shallower than the no-LWD scenario (test Pa).

4 Analysis and Discussion

4.1 Geometrical and morphological features

The results shown in the previous section have highlighted the influence that porosity of LWD accumulations can have on the resulting scour hole. Crucially, the overall effect of porosity is to reduce the size of the scour hole by a degree that is directly dependent on the magnitude of the porosity. In this study, it has been observed that maximum scour depth of porous LWD jams is on average 17% lower than non-porous accumulations, up to 50% (e.g., Figure 9). This is in contrast with observations by *Cantero-Chinchilla et al.* (2021) and *Lagasse et al.* (2010), who suggested that effects of porosity are negligible (approximately a 10% reduction), although this discrepancy may be a result of the low porosity used in their experimental study and for the small number of experiments carried out. For example, *Lagasse et al.* (2010) tested porosity at only p=0.25 and for only one type of geometry and flow. On the other hand, the results shown in the current work are in line with the observations by *Schalko et al.* (2019) that the maximum scour depth increases non-linearly with increase in solid LWD volume (i.e.,

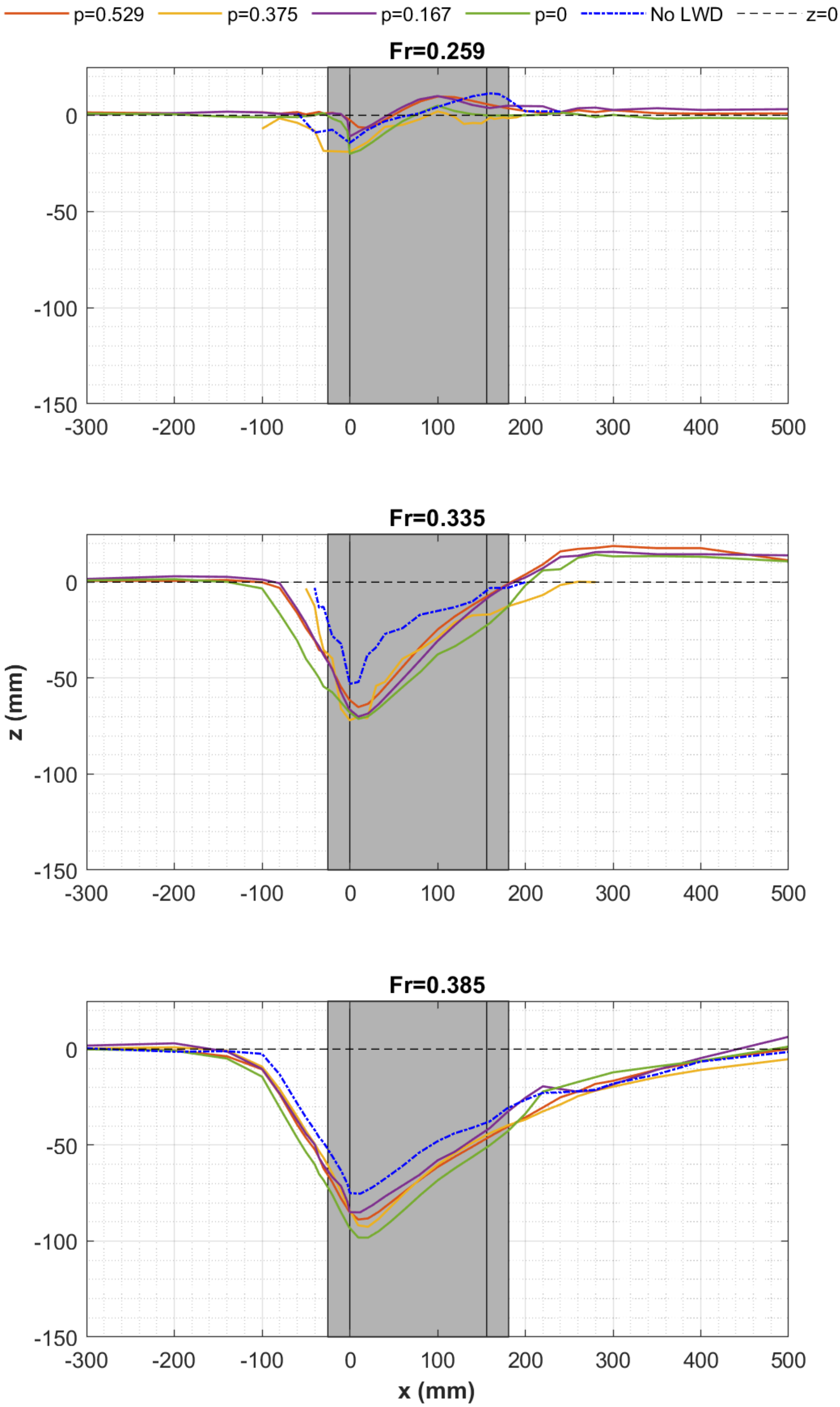

Figure 6. Longitudinal profile of scour obtained from plotting the maximum scour depth at each flow cross-section (y=0 for x <-25 mm and x >181 mm, and y=±12.5 mm in between) for LWD size A.

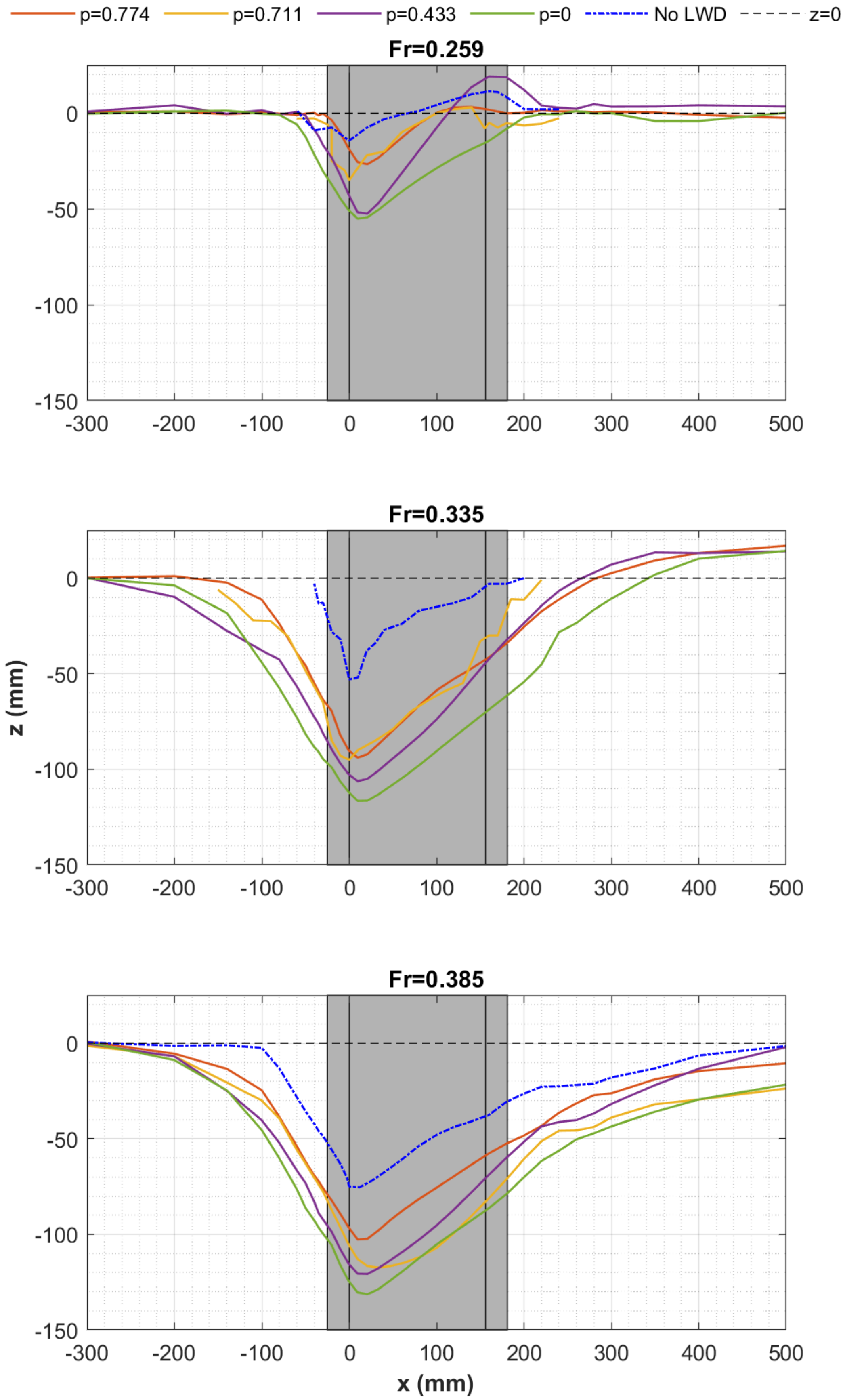

Figure 7. Longitudinal profile of scour obtained from plotting the maximum scour depth at each flow cross-section (y=0 for x <-25 mm and x >181 mm, and y=±12.5 mm in between) for LWD size D.

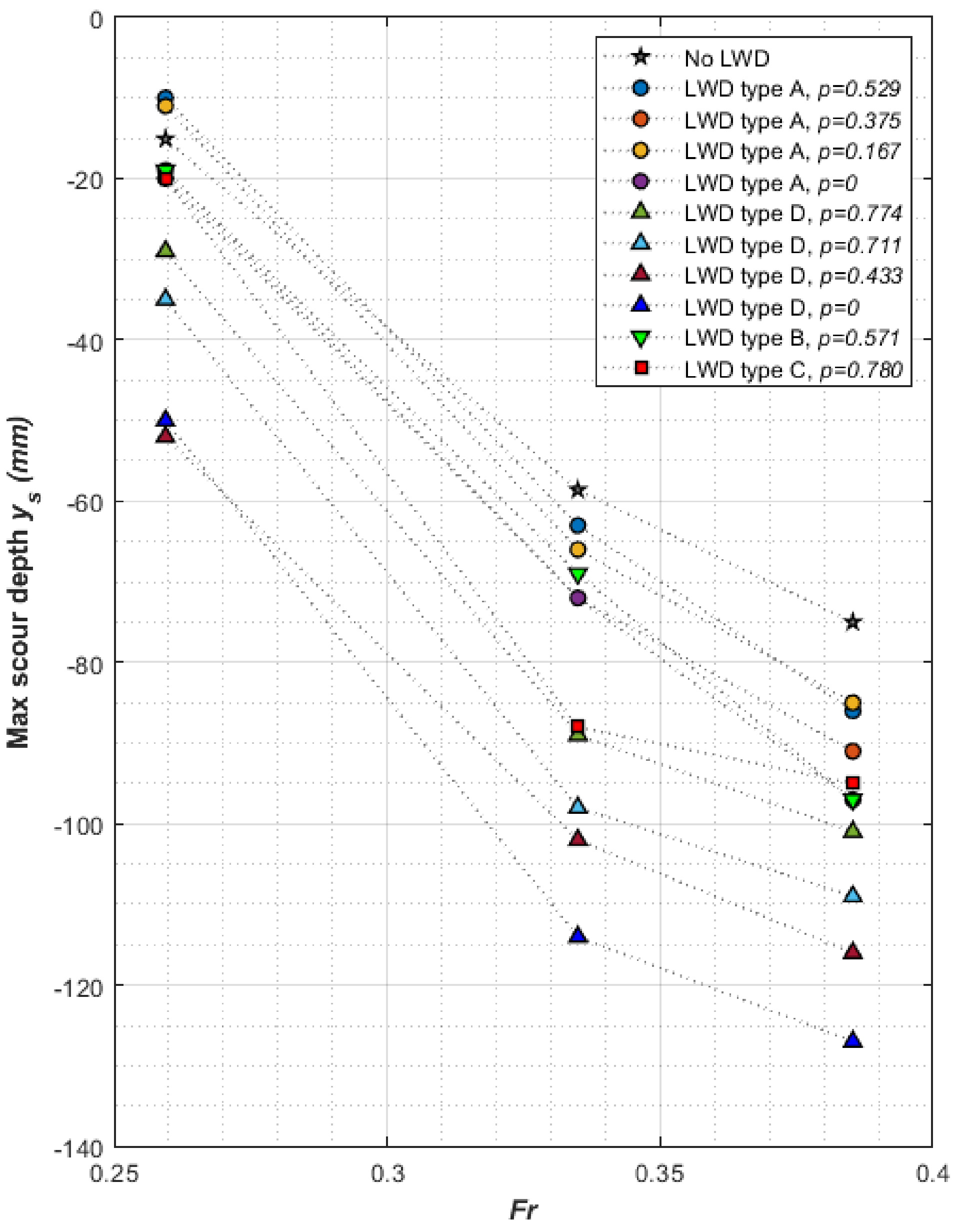

Figure 8. Maximum depth of the scour hole for all experimental tests for all tests.

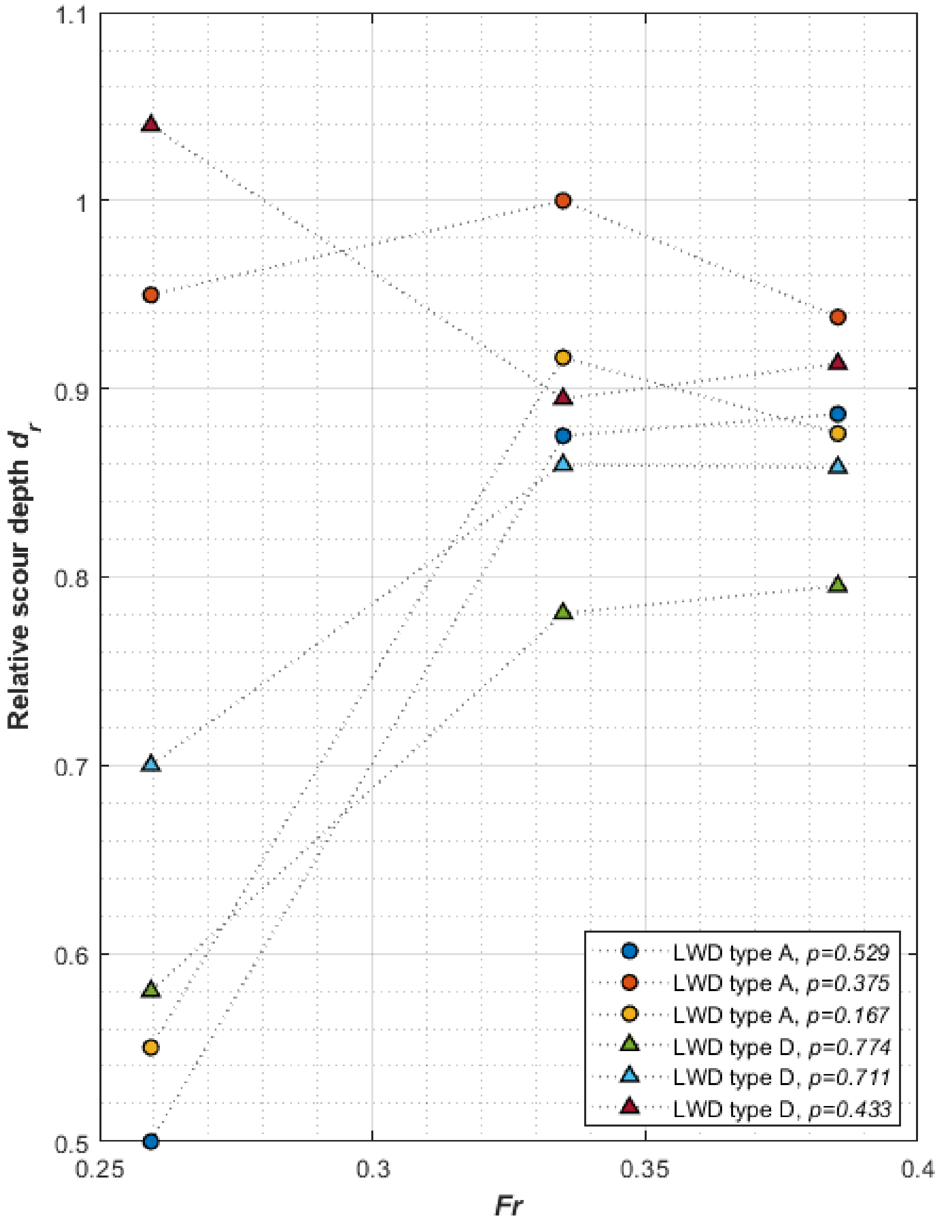

Figure 9. Relative scour depth d_r of the scour hole for LWD sizes A and D.

decrease in porosity). This is not surprising since a porous system will permit part of the fluid to flow through its structure and therefore will reduce the flow acceleration caused by the LWD obstruction. On the other hand, experimental data shown in Figures 6 to 9 suggest that this is not a linear process, i.e., the size of the scour hole does not linearly decrease with porosity across all of the observed experiments. For example, the scour hole in test A3c ($p = 0.167$) is smaller and shallower than A1c ($p = 0.529$). This discrepancy is in line with observations for vorticity systems developing beyond cylinders with different porous density immersed in flows (*Taddei et al.*, 2016) to mimic canopy patches. *Taddei et al.* (2016) observed that vertical and horizontal bleeding strongly depend on the level of porosity and play a vital role in affecting the flow wake, thus affecting the development and formation of the scour hole. Interestingly, two tests (A1a and A3a) showed maximum scour depths (and, indeed both scour hole width and depth) smaller than test Pa, i.e., a no-LWD scenario. There can be two possible explanations for this observation: either the combination of flow characteristics and LWD porosity negatively impacts scour formation by reducing the shear stress and therefore mitigating the removal of sediment; or, the observation comes as a result of the inherent stochasticity of the phenomenon. In support of the latter hypothesis, these observations only occurred with the smallest LWD jam (geometry A) for the smallest of the Fr values and in one case with the highest porosity, which may indicate that under these conditions the vorticity system at the pier is not noticeably enhanced by the LWD and hence likely to be similar to the no-LWD scenario.

Another interesting observation is related to the scour hole for the lowest values of Fr (e.g. Figure 3). For this case, the scour hole is primarily in the region $x \geq 0$, with very limited erosion (i.e., <5 mm) in the upstream front, which is in contrast with scour holes typically observed in the literature (i.e., holes forming upstream of the bridge pier), e.g. *Melville and Dongol* (1992); *Pagliara and Carnacina* (2013). The only exception is the no-LWD scenario (i.e. test Pa). This effect is most emphasised for the smallest LWD size (geometry A) having the highest porosity p. Thus, this observation may suggest that a highly porous obstruction of full-scale size comparable to LWD size A may actually develop a scour hole away from the front face of the pier, therefore with possibly beneficial effects to the scour risk of the structure. However, for higher Fr, this tendency was not observed for any of the values of p tested.

The importance of Fr for all experiments in the development and formation of the scour hole is tightly intertwined with the physical process causing sediment removal at the pier foundation. In our experiments, a change of Fr corresponded to a change of flow velocity, due to the water depth being kept constant. It is well-known that around bridge piers scour is caused by the formation of an intense vorticity system (namely, horseshoe and wake vortices) that by lifting and dragging sediment grains causes its removal from the pier foundation area (*Dargahi*, 1990; *Dey et al.*, 1995). The obstruction caused by a LWD jam causes a local acceleration and increase of flow velocity that can be substantial (*Pagliara and Carnacina*, 2013) especially in the downwards direction in the proximity of the pier. The accelerated flow will increase the bed shear stress locally, as well as intensity and extension of both horseshoe vortex and wake vortex, which will then cause more sediment to detach from the river bed and be transported downstream. This increased scour due to LWD accumulations was observed in all but two experimental tests in this work when compared to the pilot tests (i.e., pier only with no LWD, as described earlier in the text). In this context, it becomes clear that a solid obstruction (such as the impervious LWD jams experimentally tested in some works in the literature) will cause a much more important flow velocity increase than a porous solid, in which part of the fluid flow can bleed through, although not in a linear fashion, as observed for other porous systems (e.g. *Taddei et al.*, 2016). Not surprisingly, experimental results are consistent with this hypothesis, showing that impervious accumulations (i.e., p=0) have the largest and deepest scour hole for given LWD size and flow characteristics, whilst porous LWD jams have all smaller scour holes. Therefore, it is reasonable to assume that the reduction in size of the scour hole for porous LWD accumulations (when compared to solid jams) is caused by a less accelerated flow and, thus, a weaker system of vortices and reduced bed shear stress. This process is also likely to explain the formation of the dune on either side downstream of the bridge pier that occurred only for the lowest Fr value: when sediment is removed from the upstream face of the pier due to the horseshoe vortex and transported downstream, the intensity of the wake vortex and the drag force applied to the sediment grains is weak (because Fr is low); thus, the sediment fall velocity is greater than its flow-wise velocity and grains will rapidly deposit. The downstream shift of the dune location and its increase in size observed for larger and less porous jams (but still at the lowest Fr value) is likely caused by the localised acceleration of the flow velocity, which increases the scour hole locally, but due to not sufficiently strong flow is still depositing immediately downstream of the scour hole, forming the observed dunes.

An analysis of the effects of LWD porosity on the maximum scour depth can offer interesting conclusions, which also have practical applications. As previous studies (e.g. *Ebrahimi et al.*, 2018, 2020) based the estimation of maximum scour depth y_s on results from experiments using fully impervious LWD jams, they tend to be highly conservative in their predictions. To make these predictions more realistic, a factor that accounts for the effective reduction in y_s according to the LWD porosity value can be useful. In practice, this would mean rearranging Equation (3):

$$y_{s,eff} = y_{s,imp} d_r \tag{4}$$

where $y_{s,eff}$ is the effective maximum scour depth computed including the porosity of a LWD accumulation, $y_{s,imp}$ the scour depth computed for the LWD accumulation if it were assumed to be impervious (as can be estimated from past works in the literature), and d_r a factor less than 1 representing the effective percentage reduction in scour depth due to an accumulation's porosity, that is the relative scour depth as defined in Equation (3). d_r can be derived using a functional relationship that depends on the porosity of the LWD jam and other flow and LWD related parameters.

The functional relationship for d_r can be derived as follows. The first step is to perform a dimensional analysis, which can provide useful insights on the main parameters that need to be considered in such a relationship.

$$y_{s,eff} = f\left(y_{s,imp}, v, h, g, \rho, \mu, W_{LWD}, K_{LWD}, H_{LWD}, p, d_{50}\right) \tag{5}$$

where g is acceleration due to gravity, ρ is water density, μ is water viscosity, and W_{LWD}, K_{LWD} and H_{LWD} are width (along the y axis), length (along the x axis) and height (along the z axis) of the LWD accumulation, respectively, as shown in Figure 1. Quantities that are directly related to scour depth for impermeable solids, such as sediment density, pier size and shape, are not included in this analysis as they are already included in $y_{s,imp}$, and are assumed to not affect reduction in scour depth for porous LWD jams. The dimensionless form of (5) is:

$$d_r = f\left(Fr, Re, \frac{W_{LWD}}{h}, \frac{K_{LWD}}{h}, \frac{H_{LWD}}{h}, p, \frac{d_{50}}{h}\right) \tag{6}$$

where d_r is the ratio between $y_{s,eff}$ and $y_{s,imp}$ as from Equation 4, Fr is the Froude number and Re is the Reynolds number. Three assumptions have been made for this study: i) the tested flow was always within the turbulent regime (i.e. $Re \geq 33000$), therefore Reynolds invariance can be assumed at full scale and the Reynolds number relaxed from (6); ii) only a single type of grain size was tested, as well as a single value of water depth, so that the ratio d_{50}/h can be ignored. However, it should be noted that grain size might have an influence on the overall scour and, therefore, different sizes of sediment may produce different results; iii) the width W_{LWD} and length K_{LWD} of the LWD accumulation (i.e. the jam extent at the water surface) have a negligible influence on the development of the scour hole in comparison to the relative depth H_{LWD}/h; this was also observed by *Ebrahimi et al.* (2018), and therefore the terms W_{LWD}/h and K_{LWD}/h are removed from (6). As a result, a simplified version of the functional relationship in (6) is defined as:

$$d_r = f\left(Fr, \frac{H_{LWD}}{h}, p\right) \tag{7}$$

Based on the experimental data, and the results shown in the previous section, the best functional relationship obtained through a principal component analysis for (7) can be expressed as:

$$d_r = 1 - \frac{P(p)}{Fr_{rel}^2} \tag{8}$$

whereby $P(p)$ is a regression function in terms of LWD porosity p that can be estimated using the experimental data, whilst Fr_{rel} is effectively Fr with the inclusion of the relative water depth H_{LWD}/h:

$$Fr_{rel} = \frac{v}{\sqrt{g\left(h - H_{LWD}\right)}} = \frac{v}{\sqrt{gh\left(1 - \frac{H_{LWD}}{h}\right)}} \tag{9}$$

It should be noted that Equation (8) is valid for the condition $P(p) \leq Fr_{rel}^2$ (i.e., $d_r \geq 0$), otherwise it will produce negative values. In practice, this would suggest that negative values can be simply taken as d_r=0, potentially indicating that excessive porosity removes the effect of accumulated LWD, i.e., $y_{s,eff} \approx 0$. Nevertheless, situations in which $P(p) > Fr_{rel}^2$ have never been observed in this study, and therefore any application of Equation (8) should be limited within the range of Fr_{rel} and p tested in this work.

Figure 10 shows the experimental data for d_r (red circles) in relationship to the porosity p for all Fr_{rel} values. In order to provide a formulation for the regression function $P(p)$, equation (8) has been rearranged as follows:

$$P(p) = \left(1 - d_r\right) Fr_{rel}^2 \tag{10}$$

Figure 10 shows also the newly amended relationship for the regression function $P(p)$ according to (10) and plotted against porosity p. Using the measured scour depths and relative Froude number Fr_{rel} from the experimental data, the function $P(p)$ in (10) has been estimated by a non-linear regression using a non-linear least squares method and a bisquare robust weighting, which leads to:

$$P(p) = 1.412p^3 - 1.217p^2 + 0.312p \tag{11}$$

for which RMSE is 0.026 and SSE is 0.010. Figure 10 shows that $P(p)$ has a strong non-linear tendency, especially for increasing values of p; it is also expected that for p nearing 0, $P(p)$ would tend to 0 as well, hence we preferred a cubic regression that would capture this expected tendency, even though outside the range of observed values. Furthermore, the non-linear tendency of the function $P(p)$ is comparable to the trend estimated for the relative LWD volume in *Schalko et al.* (2019) although the functional relationship is defined in a different form. This is possibly due to the difference between the two studies in how porosity is considered. In our work, porosity is defined as the ratio between actual solid volume and theoretical solid volume for LWD accumulations. In contrast, *Schalko et al.* (2019) considered porosity (although not defined as such, but as relative LWD volume) as the ratio between solid LWD volume and a threshold LWD volume before a carpet of LWD begins forming upstream of the accumulation. Consequently, whilst our definition of porosity p is limited by $0 \leq p \leq 1$, the ratio employed by *Schalko et al.* (2019) can be >1. Furthermore, *Schalko et al.* (2019) formulated an equation to quantify the maximum scour depth, whilst in our work we focused on the relative scour

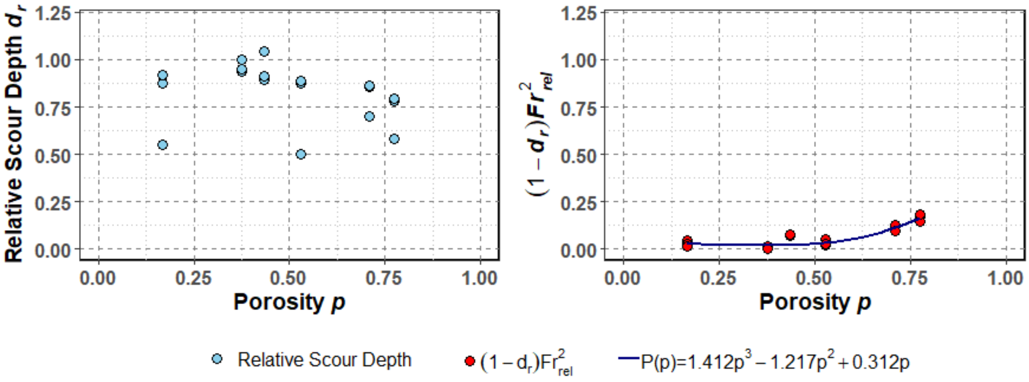

Figure 10. Values of relative scour depth d_r (left), and modified relative scour depth (right) according to equation (10) (vertical axis) against values of porosity p (horizontal axis), observed for the experimental tests. The regression function $P(p)$ is also included.

depth d_r, which is a reduction factor applied to the maximum scour depth estimated considering an impervious LWD accumulation.

Figure 11 (top) plots the predicted maximum dimensionless scour depth d_r obtained using Equation (8), versus the observed values and also the line of perfect agreement. The bottom plot in the same figure shows the predicted maximum scour depth $y_{s,eff}$ versus the observed values and also the line of perfect agreement. Both plots show that the function in Equation (8) offers a good degree of approximation when using the regression in Equation (11). The upshot of the relationships outlined in this section is that a more realistic estimation of maximum scour depth at bridge piers will be possible, instead of considering a fully solid and impervious LWD jam, which may result in an overestimation of y_s.

It is important to note that the inherent stochasticity of flume experiments with scour at bridge piers may produce errors that could impede the accuracy of prediction, such as in Equation (8). Studies such as *Schalko et al.* (2019) estimated prediction errors to be of the order of 27%, which is higher than the observed average reduction (17%) in maximum scour depth in this paper. However *Schalko et al.* (2019)'s study was for a very different scenario, which involved LWD accumulations at racks with the accumulations dynamically forming while the experiment was carried out, whereas our experiments tested static LWD jams. Nevertheless, a statistical analysis to ascertain whether the relative scour depths $d_{r,pred}$ predicted by (8) were consistent with the observed relative scour depths $d_{r,obs}$ is still useful. The Pearson's coefficient was calculated as R^2=0.82. We then conducted a paired t-test with the null hypothesis that the the true mean difference between $d_{r,pred}$ and $d_{r,obs}$ is equal to 0. The resulting p-value was 0.8983, which supported the null hypothesis, hence providing evidence that there is no significant difference between predicted and observed values. Secondly, we analysed the prediction residuals (i.e., $d_{r,obs}-d_{r,pred}$) and relative errors (i.e., $\frac{d_{r,obs}-d_{r,pred}}{d_{r,obs}}$) in a Bland-Altman plot (see Figure 12), to evaluate the agreement between observed and predicted scour depths. This figure shows the observed scour depth ($d_{r,obs}$) on the horizontal axis, whilst both residuals and relative errors are shown on the vertical axis. The red dotted line represents the mean values of both residuals and relative error, whilst the dotted blue lines indicate the limits of agreement (that are 1.96 times the standard deviation of residuals and relative error, respectively), that define the range within which most values are expected to fall. The data scattering around the mean line is in most cases random with the majority of the points clustered around the average, indicating a good agreement be-

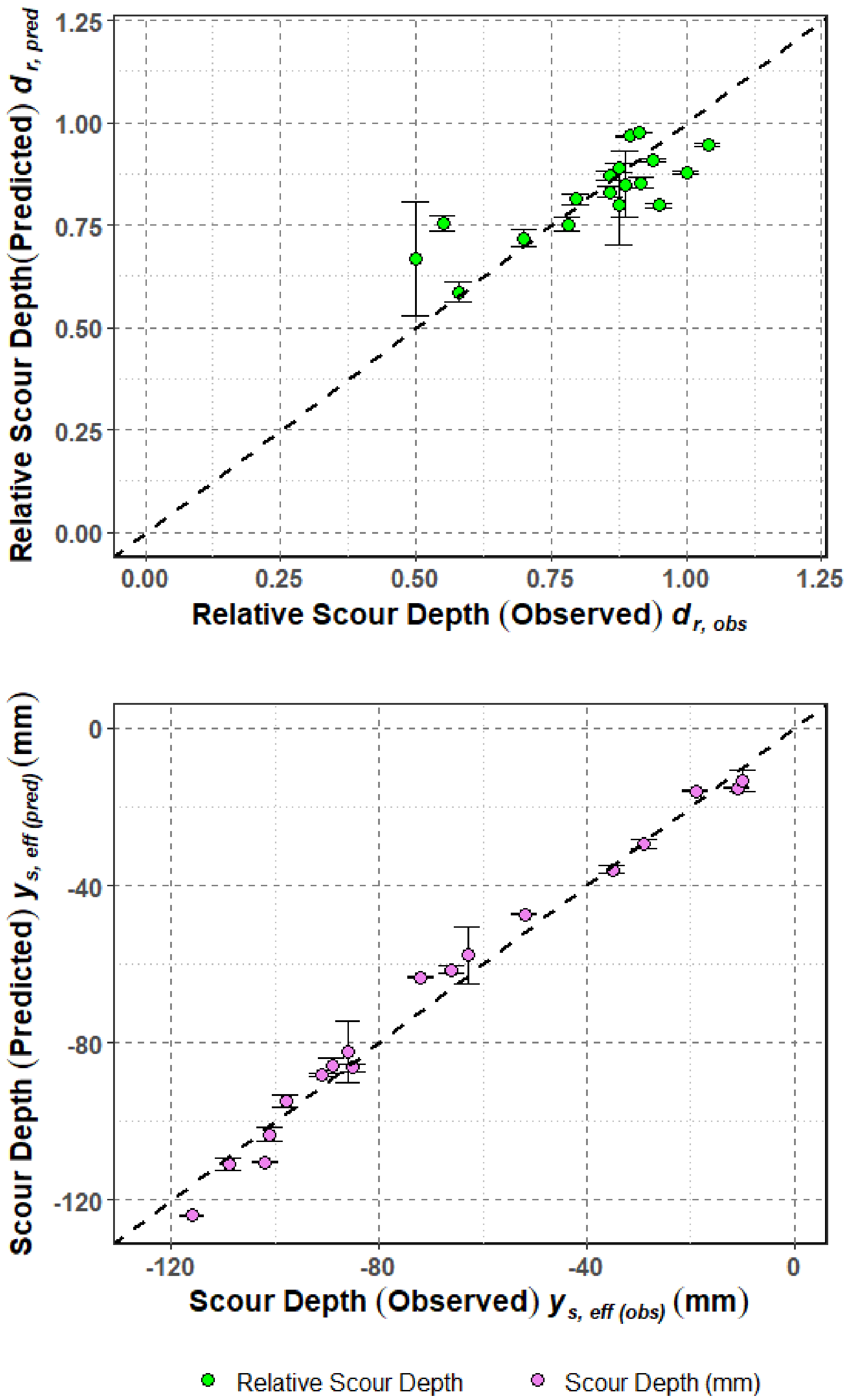

Figure 11. Comparison between (horizontal axis) observed and (vertical axis) predicted (top) dimensionless scour depth d_r, (bottom) maximum scour depth $y_{s,eff}$, with indication of the line of perfect agreement (dashed line). The figure also includes error bars calculated using (13) for error propagation analysis.

Table 3. Total errors of input variables used for estimation of total error propagation, and average total error estimation according to Equation (13)

Variable	**Total error**
Discharge ε_Q	0.0001 m^3/s
Channel width ε_B	0.002 m
Water depth ε_h	0.0005 m
LWD size $\varepsilon_{W,K,H}$	0.001 m
Relative Froude $\varepsilon_{Fr_{rel}}$	0.014
Porosity ε_p	0.058
Relative scour depth ε_y	0.036

tween $d_{r,obs}$ and $d_{r,pred}$. Thirdly, we estimated the error back-propagation, in accordance with *Schalko et al.* (2019). Back-propagation error analysis allows estimation of the propagated uncertainty based on the uncertainties associated with the input data. The generalised formula to a function y is:

$$\varepsilon_y = \sqrt{\left(\frac{\partial f}{\partial x_1}\right)^2 \varepsilon_{x_1}^2 + \left(\frac{\partial f}{\partial x_2}\right)^2 \varepsilon_{x_2}^2 ... + \left(\frac{\partial f}{\partial x_i}\right)^2 \varepsilon_{x_i}^2} \tag{12}$$

where x_1, x_2, x_i are the independent variables of such function, ε_{x_1}, ε_{x_2}, ε_{x_i} the associated uncertainty (or hereafter defined as propagated errors) for the independent variables, and ε_y the calculated uncertainty for the function y. The generalised formula, when applied to equation (8), becomes:

$$\varepsilon_y = \sqrt{\left(\frac{\partial d_r}{\partial Fr_{rel}}\right)^2 \varepsilon_{Fr_{rel}}^2 + \left(\frac{\partial d_r}{\partial p}\right)^2 \varepsilon_p^2} \tag{13}$$

where ε_y is the propagated error for d_r, $\varepsilon_{Fr_{rel}}$ and ε_p are the propagated errors for Fr_{rel} and p, respectively. $\varepsilon_{Fr_{rel}}$ and ε_p are also calculated using Equation (12) for (9) and (2), respectively. Table 3 displays the errors for each measured value within the experimental campaign, which have then been used to estimate ε_y. The resulting back-propagated error is, on average, 3.59%, which is well below the typical range of observed scour depth reduction, indicating that the estimated reduction in scour depth can confidently be attributed to porosity of LWD jams. Only two data points showed a relatively high (i.e., 20.9% and 12.6%) error, whilst first quartile, median and third quartile error values were all well below 5%, i.e., 0.5%, 1.6%, and 2.8% respectively. Figure 11 shows $d_{r,obs}$ and d_{r_pred} with inclusion of the error bars for each point, as estimated by Equation (13), as well as the dimensional values of observed and predicted scour depth $y_{s,eff}$. It can be observed that except for a few cases, errors are typically small (<5% in the majority of the cases), suggesting that uncertainty in the estimation of d_r (and, consequently, $y_{s,eff}$) is relatively small. Therefore, it can be concluded that d_r as defined in this paper is a reliable estimator of the relative scour depth, and that uncertainties are in general expected to be smaller than the effect of scour depth reduction induced by porous LWD jams. The estimated errors in our work differ from *Schalko et al.* (2019), mostly for two reasons: (i) the different experimental settings, and (ii) likely the most important, the different regression equations that have been used.

Findings from this research are applicable for scour risk assessment and bridge design in practice. For example, the relative scour factor d_r can be employed to reduce the maximum scour depth according to LWD porosity when estimating the effects of LWD on scour for a bridge pier foundation. Since existing formulae for scour estimation are

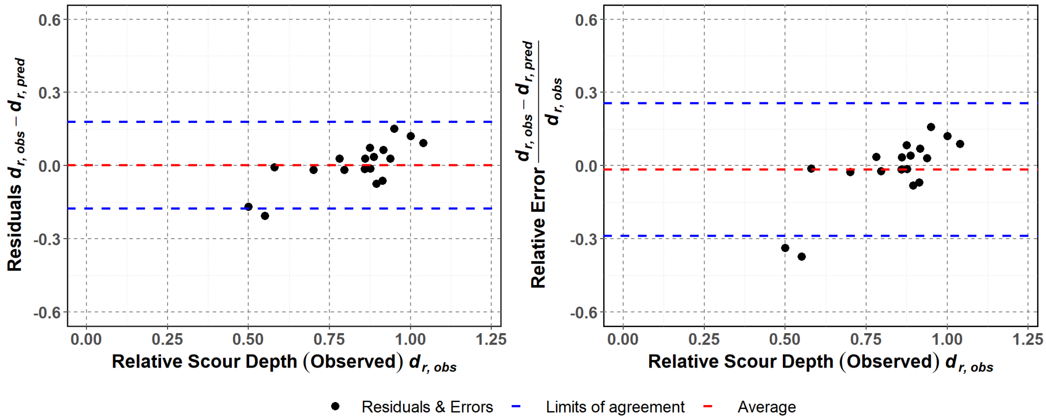

Figure 12. Bland-Altman graph of residuals (left) and relative errors (right) for observed and predicted values of relative scour depth d_r, against the observed values (horizontal axis). The blue lines represent the limits of agreement for each graph, whilst the red lines represent the average for residuals and relative errors respectively.

Table 4. Summary of existing equations for estimation of maximum scour depth at bridge piers, with inclusion of Equation (8), and range of relative scour depth d_r based on experimental data used in this paper (namely, p=0.167 - 0.780). For comparison, the range of relative scour depth obtained in our work corresponds to d_r=0.59 - 0.98.

Reference	Amended equation	d_r range
Ebrahimi et al. (2020)	$y_s = D\Phi_{shape}\Phi_{depth}\Phi_{velocity}\Phi_{angle}\Phi_{debris}d_r$	0.48 - 0.93
Melville and Dongol (1992)	$y_s = 2.4D_e d_r$	0.31 - 0.78
Lagasse et al. (2010)	$y_s = 2.0D_{eff}K_1K_2K_3K_4(h/D_{eff})^{0.35}Fr^{0.43}d_r$	0.23 - 0.87
Pagliara and Carnacina (2011)	$y_s = y_{s0}(1 + 0.036\Delta A^{1.5})d_r$	0.06 - 0.94

based on solid impervious jams, they overestimate the scour effects for a pier when applied in the real-world; the use of d_r can correct this. In fact, Equation (8) is not a novel equation for scour depth estimation, but instead one for estimating the reduction in scour depth due to the porosity of a LWD accumulation. In principle, d_r computed from this equation can be employed in conjunction with any of the equations available in literature to estimate the maximum scour depth based on experimental data obtained using impervious LWD shapes. Table 4 shows examples of such equations from existing studies based on values of H_{LWD} and Fr_{rel} comparable to this study. The equations have been modified to accommodate d_r by incorporating it as a multiplying factor. Furthermore, when d_r is computed using Equation (8) for the experimental settings that have been used in the past studies, the resulting values of d_r (Table 4) are in most cases within the range observed in this work. It should be noted that equations used in Table 4 are commonly used for estimation of scour depths with and without LWD accumulations - e.g., *Ebrahimi et al.* (2020) is adopted in the UK for estimation of scour at highway bridges with inclusion of LWD accumulations (*Takano and Pooley*, 2021) and hence outputs of the current research are also expected to have immediate application within practice. Further research is needed to investigate how LWD porosity affects scour holes for flow, sediment, and LWD size conditions that were not tested in this work. Future investigations can also focus on the influence of porosity of LWD accumulations at other kinds of in-line structures apart from single bridge piers (for example, abutments).

5 Conclusions

The accumulation of LWD at bridge piers is a phenomenon that can have catastrophic effects for the structural integrity of bridges. Whilst in recent years several studies have investigated the estimation of maximum scour depth at bridge piers in the presence of LWD, these mostly used solid, prismatic, impervious LWD accumulations. This paper instead focuses on understanding how the porosity of LWD jams influences scour hole formation from a detailed flume lab experimental campaign. It presents results from a detailed experimental campaign involving LWD accumulations with a range of porosity values and sizes, while also keeping LWD shapes similar to real-world observations. The main findings of this work are as follows:

- LWD accumulations at bridge piers (irrespective of whether they are porous or non-porous) resulted in wider and deeper scour holes (up to 3.5 times larger) than in cases without LWD except in a few cases, namely for the lowest Fr and smallest LWD size tested (possibly suggesting that the effects on scour at these conditions are negligible); these observations are consistent with past studies using prismatic non-porous jams;
- The formation and size of the scour hole depends substantially on the size of the LWD accumulation and flow characteristics. Specifically, the larger the LWD and the higher the Froude number, the larger will the scour hole be;
- Porosity of LWD accumulations plays a key role in affecting the final scour hole size. In particular, porous jams will display a maximum scour depth that is up to 50% smaller than that caused by impervious LWD accumulations, for the same size and flow conditions;
- The reduction in scour depth for different values of porosity does not follow a linear trend, instead this seems to be strongly non-linear;
- A relative depth factor d_r for the estimation of the maximum scour depth reduction for porous LWD accumulation has been proposed in this work; this relies on a non-linear regression on parameters such as LWD porosity, the Froude number Fr and the relative depth underneath the LWD jam.

The results outlined in this paper will pave the way for more realistic scour depth estimations that consider the porosity of LWD accumulations. Practical applications include scour assessment and design for hydraulic actions at bridge piers. Furthermore, this research will act as a stepping stone for future studies that evaluate the influence of porosity of LWD accumulations on scour for structures beyond single bridge piers (e.g. accumulations that span the full width of single span bridges, or at abutments).

Acknowledgments

The authors are grateful to Mr Julian Yates for material help with the flume set up, and to the student Ms Antoneta Verushi for the practical help with experimental runs. The authors are also grateful for the financial support by the UK Engineering and Physical Sciences Research Council (EPSRC) through an Impact Acceleration Award, grant number EP/R511699/1 and to the Devon County Council (UK) for the financial and material support provided for this research. The authors would like to thank the Associate Editor and two anonymous reviewers for the constructive comments that improved the quality of this paper.

6 Open Data

The data used for supporting the results presented in this paper are openly available from the University of Exeter repository at doi: https://doi.org/10.24378/exe.4744 (*Panici and Kripakaran*, 2023)

References

Benn, J (2013), Railway bridge failure during flooding in the UK and Ireland, *Proceedings of the Institution of Civil Engineers*, *166*(4), 163–170.

Cantero-Chinchilla, F.N., G.A.M. de Almeida, and C. Manes (2021), Temporal Evolution of Clear-Water Local Scour at Bridge Piers with Flow-Dependent Debris Accumulations, *Journal of Hydraulic Engineering*, *147(10)*, https://doi.org/10.1061/(ASCE)HY.1943-7900.0001920.

Dargahi, B. (1990), Controlling mechanism of local scouring, *Journal of Hydraulic Engineering*, *116(10)*, 1197–1214.

Dey, S., S.K. Bose, and G.L.N.. Sastry (1995), Clear water scour at circular piers: a model, *Journal of Hydraulic Engineering*, *121(12)*, 869–876.

Diehl, T.H. (1997), Potential drift accumulation at bridges, Federal Highway Administration, U.S. Department of Transportation, Washington D.C., USA.

Ebrahimi, M., P. Kripakaran, D. Prodanovic, R. Kahraman, M. Riella, G. Tabor, S. Arthur, and S. Djordjević (2018), Experimental study on scour at a sharp-nose bridge pier with debris blockage, *Journal of Hydraulic Engineering*, *144*.

Ebrahimi, M., S. Djordjević, D. Panici, G. Tabor, and P. Kripakaran (2020), A Method for Evaluating Local Scour Depth at Bridge Piers due to Debris Accumulation, *Proceedings of the Institution of Civil Engineers - Bridge Engineering*, https://doi.org/10.1680/jbren.19.00045.

Garde, R.J. (1970), Initiation of motion on a hydrodynamically rough surface, critical water velocity approach, *Journal of Irrigation Power*, *27*, 271–282.

Gurnell, A.M., and J. England, and L. Burgessgamble (2019), Trees and wood: working with natural river processes, *Water and Environment Journal*, *33*, 342–352.

Lagasse, P., P. Colopper, L. Zevenbergen, W. Spitz, and L. Girard (2010), Effects of debris on bridge pier scour, National Cooperative Highway Research Program, Transportation Research Board, Washington D.C., USA.

Laursen, E.M., and A. Toch (1956), Scour around bridge piers and abutments, Iowa Institute of Hydraulic Research, Iowa Highway Research Board, Iowa City, USA.

Livers, B., K.B. Lininger, N. Kramer, and A. Sendrowski (2020), Porosity problems: Comparing and reviewing methods for estimating porosity and volume of wood jams in the field, *Earth Surface Processes and Landforms*, *45*, 3336–3353.

Lyn, D., T. Cooper, Y. Yi, R. Sinha, and A. Rao (2003), Debris accumulation at bridge crossing: Laboratory and field studies, Federal Highway Administration, U.S. Department of Transportation, Washington D.C., USA.

Lyn, D., T. Cooper, C. Condon, and G. Gan (2007), Factors in debris accumulation at bridge piers, Federal Highway Administration, U.S. Department of Transportation, Washington D.C., USA.

Melville, B.W., and D. Dongol (1992), Bridge pier scour with debris accumulation, *J. Hydraul. Eng.*, *118*, 1306–1310.

Melville, B.W., and Y.M. Chiew (1999), Time Scale for Local Scour at Bridge Piers, *Journal of Hydraulic Engineering*, *125(1)*, 59–65.

Neill, C.R. (1968), Note on initial movement of coarse uniform bed-material, *Journal of Hydraulic Research*, *6*, 173–176.

Oliveto, G., and W.H. Hager (2005), Further Results to Time-Dependent Local Scour at Bridge Elements, *Journal of Hydraulic Engineering*, *131(2)*, 97–105.

Pagliara, S., and I. Carnacina (2010), Temporal scour evolution at bridge piers: effect of wood debris roughness and porosity, *Journal of Hydraulic Research*, *48(1)*, 3–13.

Pagliara, S., and I. Carnacina (2011), Influence of wood debris accumulation on bridge pier scour, *Journal of Hydraulic Engineering*, *137*, 254–261.

Pagliara, S., and I. Carnacina (2013), Bridge pier flow field in the presence of debris accumulation, *Proceedings of the Institution of Civil Engineers - Water Management*, *166*, 187–198.

Panici, D., and G.A.M. de Almeida (2018), Formation, growth, and failure of debris jams at bridge piers, *Water Resources Research*, *54*, https://doi.org/10.1029/2017WR022177.

Panici, D., and G.A.M. de Almeida (2020b), Influence of pier geometry and debris characteristics on wood debris accumulations at bridge piers, *Journal of Hydraulic Engineering*, DOI: 10.1061/(ASCE)HY.1943-7900.0001757.

Panici, D., P. Kripakaran, S. Djordjević, and K. Dentith (2020), A practical method to assess risks from large wood debris accumulations at bridge piers, *Science of the Total Environment*, *728*, DOI: 10.1016/j.scitotenv.2020.138575.

Panici, D., and P. Kripakaran (2022), Assessing and mitigating risks to bridges from large wood using satellite imagery, *Proceedings of the Institution of Civil Engineers – Bridge Engineering*, DOI: 10.1680/jbren.21.00059.

Panici, D., and P. Kripakaran (2023), Scour depth for porous large woody debris accumulations at single bridge piers, https://doi.org/10.24378/exe.4744 [Dataset].

Parola, A.C., C.J. Apelt, and M.A. Jempson (2000), Debris Forces on Highway Bridges, National Cooperative Highway Research Program, Transportation Research Board, Washington D.C., USA.

Raudkivi, A.J., and R. Ettema (1985), Clear-water scour at cylindrical piers, *Journal of Hydraulic Engineering*, *109(3)*, 338–350.

Raudkivi, A.J., and R. Ettema (1985), Scour at cylindrical bridge piers in armored beds, *Journal of Hydraulic Engineering*, *111(4)*, 713–731.

Schalko, I., C. Lageder, L. Schmocker, V. Weitbrecht, and R.M. Boes (2019), Laboratory Flume Experiments on the Formation of Spanwise Large Wood Accumulations: Part II—Effect on local scour, *Water Resources Research*, *55*, 4871–4885.

Takano, H., and M. Pooley (2021), New UK guidance on hydraulic actions on highway structures and bridges, *Proceedings of the Institution of Civil Engineers - Bridge Engineering*, *174(3)*, 231–238.

Taddei, S., C. Manes, and B. Ganapathisubramani (2016), Characterisation of drag and wake properties of canopy patches immersed in turbulent boundary layers, *Journal of Fluid Mechanics*, *798*, 27–49.

Wohl, E., N. Kramer, V. Ruiz-Villanueva, D.N. Scott, F. Comiti, A.M. Gurnell, H. Piegay, K.B. Lininger, K.L. Jaeger, D.M. Walters, and K.D. Fausch (2019), The natural wood regime in rivers, *BioScience*, *69(4)*, 259–273.